Наносистеми, наноматеріали, нанотехнології
Nanosistemi, Nanomateriali, Nanotehnologii
2026, т. 24, № 1, сс. 211–224
https://doi.org/10.15407/nnn.24.01.0211

PACS numbers: 07.07.Df, 78.20.Ci, 78.66.Li, 79.20.Ds, 81.15.Fg, 81.16.Mk, 87.85.fk

Synthesis and Characterization of Nano-CdO:SnO_2 Thin Film for Gas-Sensing Applications

Huda Saadi Ali[1] and Zuheer N. Majeed[2]

[1]*College of Energy and Environmental Sciences,*
Department of Renewable Energy,
Al-Karkh University of Science,
Baghdad, Iraq
[2]*College of Education for Women,*
Kirkuk University,
Kirkuk, Iraq

Motivated by the utility of gas-sensing technology, investigations of thin films of the tin oxide-doped cadmium oxide (CdO:SnO_2) of nanograin size in the range between 10.3 nm and 18.3 nm have been undertaken applying different characterization methods. CdO films doped with nano-SnO_2 contents in the range of 1–3% were deposited on soda lime glass (SLG) substrates at room temperature by pulsed laser deposition (PLD) and succeeded by annealing for 60 min at a temperature of 400°C. The dominant phase for these films shows a hexagonal crystal structure, which is the metastable phase of the doped CdO. Tauc's relation is used for determining the energy band gap (E_g) regarding doped CdO thin films over the photon energy range of 300 nm to 800 nm. A rise in SnO_2 concentrations is accompanied by a reduction in optical transmittance. The Hall effect measurement demonstrates the *n*-type conductivity of our produced films. When the SnO_2 content is of $\cong 0.01$ and the operating temperature is of 300°C, the maximum attainable sensitivity of CdO:SnO_2 mixed films toward nitrogen dioxide (NO_2) gas is achieved in terms of sensing characteristics. The outcomes demonstrate that, with a recovery time of 60 seconds and a response time of 25 seconds, the maximum sensitivity is equivalent to 78.05%. From room temperature to 300°C, the resistance to NO_2 gas is reduced linearly with operating temperature.

Мотивовані корисністю технології газового зондування, дослідження тонких плівок оксиду Кадмію, леґованого оксидом Стануму (CdO:SnO_2), з нанорозміром зерен у діяпазоні від 10,3 нм до 18,3 нм були проведені з використанням різних методів характеризації. Леґовані плівки CdO із вмістом наночастинок SnO_2 у діяпазоні 1–3% були осаджені на підкладинках зі скла з натронного вапна за кімнатної температури методом

імпульсного лазерного осадження з подальшим відпалом упродовж 60 хвилин за температури у 400°C. Домінувальна фаза для цих плівок має гексагональну кристалічну структуру, яка є метастабільною фазою й леґованого CdO. Таукове співвідношення було використано для визначення ширини забороненої зони (E_g) для леґованих тонких плівок CdO в діяпазоні енергій фотонів від 300 нм до 800 нм. Збільшення концентрації ії SnO_2 супроводжується пониженням оптичного пропускання. Міряння Голлового ефекту демонструє *n*-тип провідности виготовлених плівок. Коли вміст SnO_2 становить $\cong 0{,}01$, а робоча температура — 300°C, досягається максимально досяжна чутливість змішаних плівок CdO:SnO_2 щодо газоподібного діоксиду Нітроґену (NO_2) з точки зору характеристик чутливости. Результати показують, що за часу відновлення у 60 секунд і часу відгуку у 25 секунд максимальна чутливість еквівалентна 78,05%. Від кімнатної температури до 300°C стійкість щодо газоподібного NO_2 лінійно зменшується з робочою температурою.

Key words: transparent metal oxide, nanothin film, pulse laser deposition, CdO, SnO_2, gas-sensing application.

Ключові слова: прозорий оксид металу, нанотонка плівка, імпульсне лазерне осадження, CdO, SnO_2, застосування в газовій сенсориці.

(Received 26 September, 2024; in revised form, 20 November, 2024)

1. INTRODUCTION

Metal peroxides are interesting since they could be employed as sensors [1], catalysts [2], sources of oxygen in organic synthesis [3], and precursors for metal-oxides' synthesis [4–6]. There are numerous ways to make metal peroxides [6], such as the direct route reaction of oxygen with metal in air (or ammonia) as well as in liquid, the reaction regarding a metal salt with hydrogen peroxide, typically in basic solution, the thermal decomposition of the superoxide, and the electrochemical route. Unfortunately, the majority of currently used techniques have some drawbacks. These include hazardous and complex fabrication processes, costly and difficult-to-find precursors, and poorly crystallized or even impure final products. The automotive industry as well as environmental research in both outdoor and indoor settings, like greenhouse gas monitoring, are only two of the many uses for gas-sensing technologies [1–6].

People are currently aware of the environmental damage caused by industrial emissions. One of such waste gases, NO_2, was linked to an increased risk of developing respiratory diseases in people, including pulmonary edema and asthma, and has raised concerns about environmental pollution on a global scale [7]. Yet, human beings cannot survive in an environment with 3 ppm NO_2 for more than 8 hrs, according to the Health and Safety Rule Alarm [8].

Lately, researchers and industry have become more interested in gas-sensing technology as a common application for intelligent devices. Researchers were exploring a range of options to improve gas-sensing performance because of the limitations and wide range of applications of numerous gas-sensing technologies. Numerous elements, including selectivity, sensitivity, response time, cost, and size, must be taken into account in order to evaluate the effectiveness of gas-sensing systems. A repeatable and stable gas signal throughout time should be shown by gas sensors as well, but structural alterations, composition, appropriate doping materials, and application of the right surface treatment all affect stability [9].

Techniques for gas sensing include liquid chromatography, gas chromatography, electrochemical sensors, acoustic sensors, optical sensors, and chemical resistance sensors. Some of these techniques, for instance, gas and liquid chromatography, and acoustic sensors have limitations of high cost, low sensitivity, slow response, and difficulty in downsizing [10–16]. On the other hand, gas sensors depend on chemical resistance of such polymers, carbon nanotubes, and metal oxide-based sensors have been used to minimize the size of a powerful and cheap device. Among these three types, metal oxides are the most popular type due to their brilliant properties [17–20].

Transparent conducting metal oxides (TCO), like tin oxide (SnO_2), indium oxide (InO), cadmium oxide (CdO), and zinc oxide (ZnO), have been investigated intensively in the last decade. CdO has attracted greater attention than other potential TCO due to its various advantages such as high carrier concentrations and moderate electron mobility [21]. These properties of CdO thin films facilitate its inclusion in different applications such as photodiodes, transparent electrodes, solar cells, and gas sensors [22]. CdO thin films crystallize as a cubic crystal system, and the dominant phase for CdO films exhibits the rock-salt crystal structure, which is the stable phase of CdO [23, 24], but it can also crystallize in metastable phases such as zinc blende, wurtzite, CsCl, and NiAs crystal structure [25]. Polycrystalline CdO thin films could be deposited through various methods, such as metal-oxide chemical vapour deposition (MOCVD), direct current sputtering (DCS) and radio-frequency sputtering (RFS), spray pyrolysis, chemical bath, and pulsed laser deposition (PLD). However, to deposit stoichiometric and tin-doped CdO, PLD is considered as the preferred method [25].

This work aims to find a correlation between the optical, structural, and electrical properties regarding doped CdO thin films with different SnO_2 contents. It is also an attempt to optimize the SnO_2 content for the best sensing ability using crystal structure, grain size, transmission, band gap, carrier concentration, mobility, and sensing characteristics for NO_2 sensing applications.

2. EXPERIMENTAL WORK

Samples were prepared using high-purity cadmium oxide (CdO) powder (99.99%) that was doped with tin oxide (SnO_2) of 99.8%. Samples weighing 3 gm, one of them pure CdO and three samples doped with SnO_2 with impurity percentages of 2, 4, 6% were weighed with a sensitive electronic balance with four decimal places after sorting from. The mixing technique has been utilized for obtaining high homogeneity between the pure CdO granules and the samples doped with SnO_2, where the powders were ground using a ceramic mortar for half an hour; then, the ground powders were placed in plastic boxes containing three balls with a diameter of 0.50 cm. After that, each box was placed inside an English type mixer (Spex) for ten minutes, and then, the mixed powders were compressed with a pressure force of 6 Tons in a special mould (steel stainless) with a diameter of 1.2 cm and a thickness of 0.3 cm for a period of 5 minutes using an American-made hydraulic press manufactured by Across International, as shown in Fig. 1.

To produce CdO tablets before and after doping, we used glass slides as substrates for film growth after cutting them into smaller pieces. To ensure their cleanliness, such glass slides are precleaned through ethanol and distilled water. Subsequently, the glass slides undergo ultrasonic cleaning. Sedimentation system consists of two parts as follow.

1. Laser System. The pulsed Nd:YAG laser manufactured by the company DIAMON-288 pattern EPLS System with a wavelength of 1064 nm, as can be seen in Fig. 2, was used in the process of depositing the prepared patterns on glass bases. The system consists of a power supply and a control system. Using a computer and an internal cooling system, the path of the laser beams is fixed on the target manually, as the laser used has the following specifications: laser energy of 100–1000 mJ (energy used is of 600 mJ); frequency 6–1 Hz (frequency used is of 6 Hz); laser wavelength $\lambda = 1064$ nm; duration of each pulse = 10 nsec and a number of 100 pulses at room temperature, as the incident laser rays create an angle of 45° with the surface of the target. Cooling method for the device: it is by manually circulating the device hot water with cold water through a tank located inside the device.

2. Sediment Chamber. It is a cylindrical chamber with a diameter of 30 cm and a height of 40 cm made of quartz. The film deposition process takes place in it, using a pulsed laser at high discharge, and it is designed to contain a gate for the gas to escape upon discharge and for viewing the laser rays.

The process of deposition of samples prepared from CdO discs before and after doping with SnO_2 took place inside the vacuum

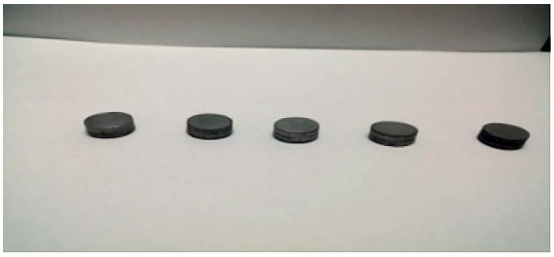

Fig. 1. Shape of the samples.

Fig. 2. The Nd:YAG pulsed laser instrument.

chamber of the laser system and under a vacuum pressure of 10^{-2} hPa. The deposition process includes basic steps, which are the interaction regarding pulsed laser beams with target, which is a compressed powder disk. Subsequently, the prepared thin films were annealed at a temperature of 400°C.

At room temperature, the experiments have been carried out with CuK_α radiation source ($\lambda = 1.5414$ Å) at 2θ-values ranging between 20 and 80 for recording the XRD data. An accelerating voltage of 30 kV and emission current of 20 mA were used in the experiment. UV–Vis spectrophotometry (UV-265 Shimadzu) was used to examine the optical characteristics of CdO:SnO_2 thin films inside the wavelength range of 300–1100 nm. A test of a gas sensor with a bias voltage of 6 V has been carried out at various sensing temperatures. With the use of aluminium electrodes for each measurement, Hall coefficient was determined utilizing a four-probe approach. Through introducing a magnetic field perpendicular to the membrane surface, Hall effect has been computed. Additionally, the Hall probability (μ_H) of electrical conductivity (σ) and the concentration of charge carriers (p) have been ascertained. Furthermore, the test was run under a bias voltage of 6 V specifically for NO_2 gas and at multiple sensing temperatures for the gas sensor measurement.

3. RESULTS AND DISCUSSION

3.1. The Crystal Structure: X-Ray Diffraction Analysis

The x-ray diffraction results of all mixed CdO:SnO_2 thin films deposited on glass substrates through PLD method and annealed at 400°C are illustrated in Fig. 3. The observed peaks include (110), (104), (111), (101), (220), (200), (311), and (222). The dominant plane is (111), which is attributed to its stability. The samples consist of a film comprising a mixture of the cubic structure of cadmium oxide and the polycrystalline structure of tin oxide with a tetrahedral arrangement [26, 27]. It can be observed that increasing the weight ratio results in an increase in the intensity regarding thin films.

Additionally, there is a reduction in full width at half maximum (*FWHM*) from 0.704 nm to 0.4257 nm in the (111) direction, indicating that the crystallite size increases from 11.8 nm to 18.3 nm for the thin film (Table) [28].

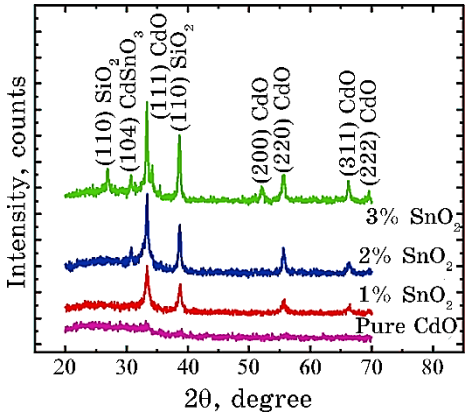

Fig. 3. XRD patterns of pure CdO and nanocomposite $CdO_{1-x}SnO_{2(x)}$.

TABLE. XRD parameters for CdO:SnO_2 thin films.

Sample	2θ, degree	*FWHM*, degree	$d_{hkl\ exp}$, Å	Grain size, nm	*hkl*
Pure	33.1539	0.8048	2.6999	10.3	(111)
1%	33.3551	0.7042	2.6841	11.8	(111)
2%	33.4054	0.5784	2.6802	14.3	(111)
3%	33.3551	0.4527	2.6841	18.3	(111)

3.2. Optical Properties

3.2.1. Transmission (T)

Figure 4 presents the optical transmittance spectra of CdO:SnO_2 thin films within wavelengths ranging from 300 nm to 800 nm and with SnO_2 contents of 0.01%, 0.02%, and 0.03%. It could be indicated that the transmittance is gradually increased with the increase in wavelength, albeit at a small rate. However, for wavelengths below 400 nm, a sharp decrease in transmittance is observed that is associated to the absorption edge in the corresponding wavelength region [29].

In the visible region, the transmittance spectrum shows a gradual increase, reaching a maximum transparency of approximately 77% in the near-infrared (NIR) region. This behaviour reflects the nature of the film. It could be attributed to an increase in oxygen content in the material or the scattering of photons by crystal defects [30]. Overall, optical transmittance decreases with an increase in SnO_2 content.

3.2.2. Optical Energy Band Gap

A critical optical constant used in fabrication of many electrical devices, depending on semiconductor physics, is the energy band gap, which is specified as the energy needed to transfer an electron from valence band maxima to the conduction band minima. The relationship (1) could be used to compute the energy gap value (E_g) [31]:

$$\alpha h\nu = A\left(h\nu - E_g\right)^r, \tag{1}$$

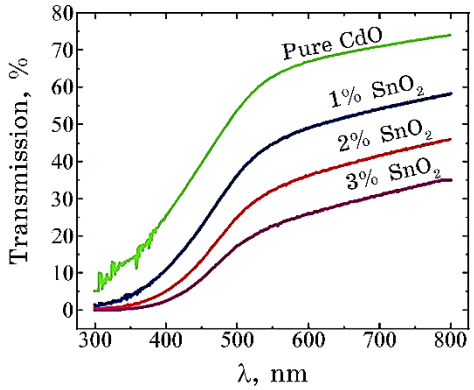

Fig. 4. Transmission of CdO thin films with different SnO_2 contents as a function of the wavelength.

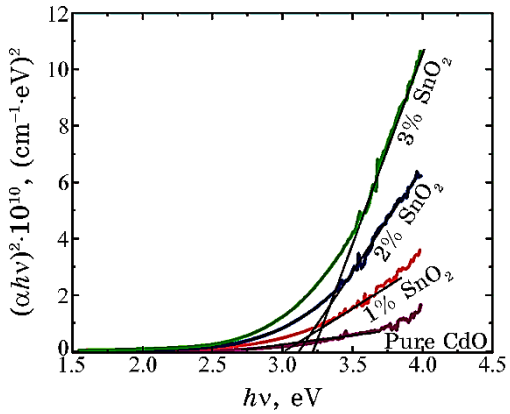

Fig. 5. Energy gap of CdO thin films with different SnO_2 contents.

in which α represents the absorption coefficient, ν represents the photon energy, A represents a constant, and r is an exponential index with a value of 1/2. By squaring Eq. (1), we obtain the following equation:

$$(\alpha h\nu)^2 = A^2(h\nu - E_g)\,. \tag{2}$$

Doping results in decreased energy-gap values, especially at higher weight ratios (Fig. 5). The energy gap is impacted by the increased doping ratios because they cause new localized states to form inside the band gap and tail states to form close to the band edges [32].

3.3. Electrical Properties: Hall Effect

Several electrical characteristics of the prepared samples are ascertained by means of the Hall-effect measurement. For nanocomposite films, carrier concentration, μ_H, conductivity, mobility, and the majority charge-carrier types are examined [33].

The electrical conductivity of a material is influenced by the concentration and mobility of the carriers, both of which are affected by temperature and impurities.

Figure 6 shows that the increase in the SnO_2 contents from 0.01 to 0.03 results in an increase in carrier concentration of the prepared thin films from $1.50 \cdot 10^{15}$ to $1.89 \cdot 10^{15}$ cm^{-3}. On the other hand, the behaviour of carrier mobility shows the opposite trend, where the increase of the SnO_2 content reduces the value of the carrier mobility from ≅ 2000 to 800 $cm^2/(V \cdot sec)$, as depicted in Fig. 6. Results are in good agreement with Ocak *et al.* [29].

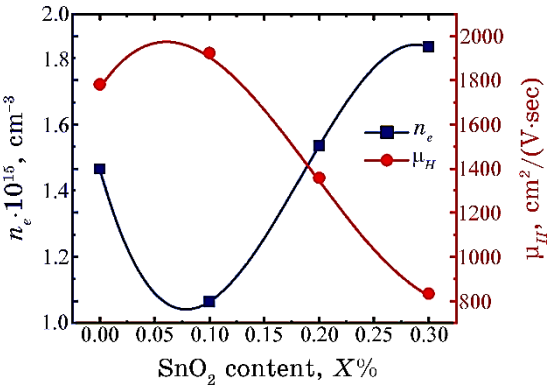

Fig. 6. Variation of n_e and μ_H with different weight ratio for CdO:SnO_2.

3.4. Gas-Sensing Properties

Two factors affect the sensors' response: the rate, at which gas molecules diffuse to the surface, and the kinetics of chemical processes taking place outside the grains. The varying rates of such processes set a limit on the sensor response at different temperatures. The maximum sensor response is achieved at intermediate temperatures, when the rates of both processes equalize. According to this process, the sensor response peaks for each gas at a particular temperature [34].

Figure 7, *a*–*d*, *e*–*h*, *i*–*l*, *m*–*p* illustrates the variation of resistance with time for the films at different operating temperatures in the case, when exposed to NO_2 gas. Gas-on period is indicated by the red arrow, while the gas-off period is shown by the green arrow. It is well known that NO_2 gas is oxidative in nature. The resistance to NO_2 gas exhibits a linear decrease with increasing temperature within the range of room temperature to 300°C.

The sensitivity regarding the sensor to NO_2 gas exhibits a linear increase with temperature within the range of room temperature to 300°C. This relationship is illustrated in Fig. 8. The maximum sensitivity of prepared CdO:SnO_2 thin films towards nitrogen dioxide (NO_2) gas is achieved, when the SnO_2 content is of 0.01. This optimal operating condition occurs at a temperature of 300°C. At this point, the maximum sensitivity reaches 78.05%. The recovery time of the sensor is of 60 seconds and response time is of 25 seconds.

When a reducing or oxidizing gas is introduced, a gas-sensor response time is the amount of time, which the sensor takes to achieve 90% of its minimum or maximum conductance value. Comparably, recovery time is the amount of time needed for the sensor to stabilize within 10% of its original baseline following the stop-

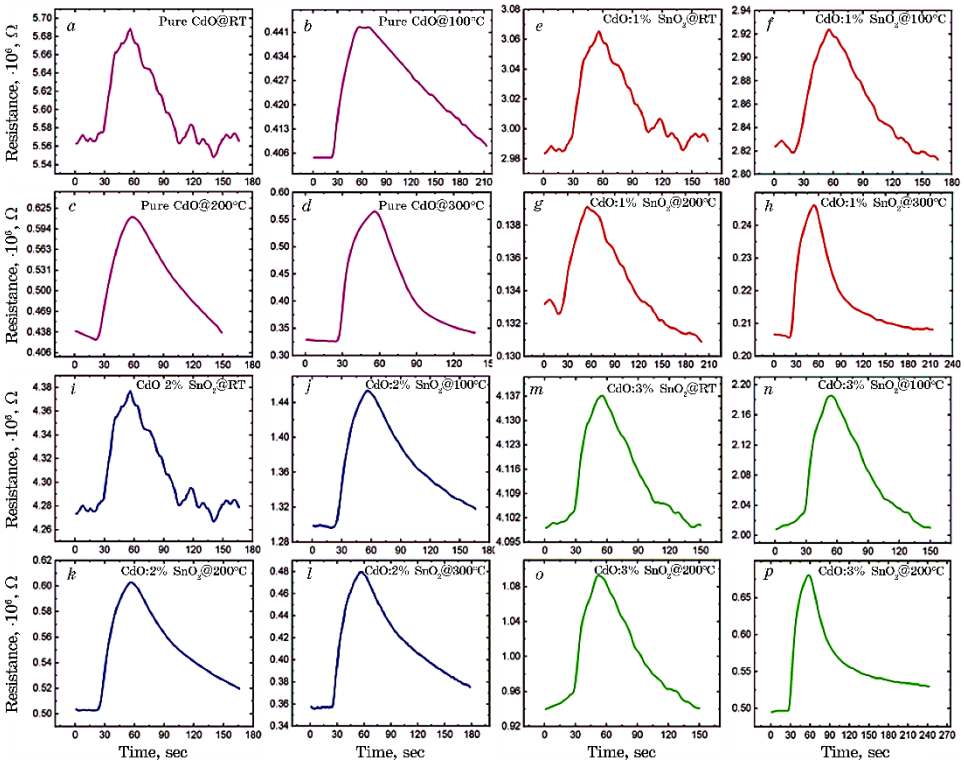

Fig. 7. Resistance variation: (*a*, *b*, *c*, *d*) for pure CdO, (*e*, *f*, *g*, *h*) for CdO:1% SnO_2, (*i*, *j*, *k*, *l*) for CdO:2% SnO_2, and (*m*, *n*, *o*, *p*) for CdO:3% SnO_2 thin films with different operating temperatures for NO_2 gas.

ping of the reducing or oxidizing gas flow [35, 36].

Figures 9 and 10 depict the relation between recovery time and response time at different operating temperatures and etching times for pure CdO and its combinations with 1%, 2%, and 3% SnO_2 (CdO:SnO_2). It is observed that the response time is fast (of approximately 20 seconds), while the recovery time is also fast (of approximately 40 seconds).

4. CONCLUSIONS

Using the PLD approach, nano-CdO:SnO_2 thin films of different compositions have been successfully formed on glass substrates. The films with the CdO:SnO_2 compositions have a polycrystalline structure, as shown by XRD analysis. As the weight ratio of SnO_2 rises, the energy gap shrinks, suggesting a trend towards lower energy levels. Thin films demonstrated the behaviour of an *n*-type charge

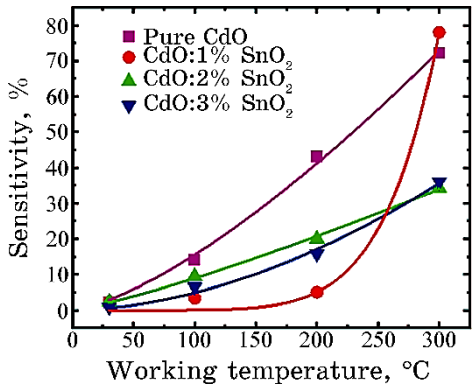

Fig. 8. Sensitivity of CdO:SnO_2 thin film towards NO_2 gas under various temperatures with different SnO_2 contents measured under various operating temperature.

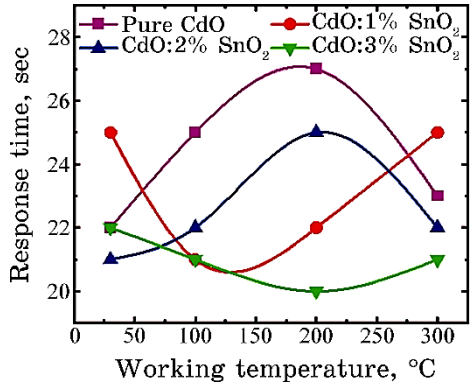

Fig. 9. Response time of CdO:SnO_2 thin films towards NO_2 gas with different SnO_2 contents measured under various operating temperature.

carrier. There appears to be an inverse link between temperature and resistance since the resistance to nitrogen dioxide reduces linearly with rising temperature. With the exception of one particular instance, the sensor sensitivity to NO_2 gas rises linearly with temperature, suggesting a positive association between the both magnitudes. Both pure CdO and mixed CdO:SnO_2 films show high resistivity at high temperatures in the case, when measuring NO_2 gas with the gas sensor, indicating lower sensitivity to NO_2 gas.

AUTHORS' NOTE

The manuscript authors affirm that they have no conflicting inter-

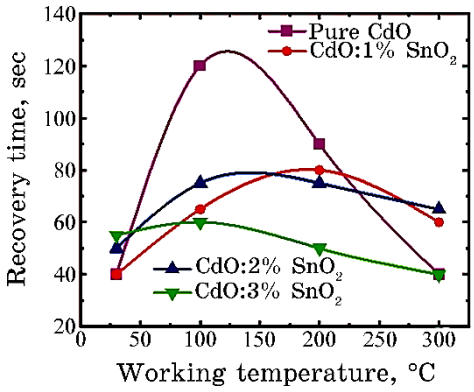

Fig. 10. Recovery time of CdO:SnO_2 thin films towards NO_2 gas with different SnO_2 contents measured under various operating temperature.

ests with publishing this work. The manuscript writers attest to its lack of plagiarism.

REFERENCES

1. M. Hulko, I. Hospach, N. Krasteva, and G. Nelles, *Sensors*, **11**, No. 6: 5968 (2011); https://doi.org/10.3390/s110605968
2. D. Lazik, S. Ebert, M. Leuthold, J. Hagenau, H. Geistlinger, *Sensors*, **9**, No. 2: 756 (2009); https://doi.org/10.3390/s90200756
3. G. F. Fine, L. M. Cavanagh, A. Afonja and R. Binions, *Sensors*, **10**, No. 6: 5469 (2010); https://doi.org/10.3390/s100605469
4. J. Zhang, J. Q. Hu, F. R. Zhu, H. Gong, and S. J. O'Shea, *Sensors*, **3**, No. 10: 404 (2003); https://doi.org/10.3390/s31000404
5. I. C. Chen, S. S. Lin, T. J. Lin, C. L. Hsu, T. J. Hsueh, and T. Y Shieh, *Sensors*, **10**, No. 4: 3057 (2010); https://doi.org/10.3390/s100403057
6. G. Coulby, A. Clear, O. Jones, and A. Godfrey, *International Journal of Environmental Research and Public Health*, **17**, No. 11: 3995 (2020); doi:10.3390/ijerph17113995
7. P. Biswas, C. Zhang, Y. Chen, Z. Liu, S. Vaziri, W. Zhou, and Y. Sun, *Biosensors*, **11**, No. 9: 326 (2021); https://doi.org/10.3390/bios11090326
8. Y. H. Navale, S. T. Navale, M. A. Chougule, N. S. Ramgir, and V. B. Patil, *Journal of Materials Science: Materials in Electronics*, **32**, No. 7: 18178 (2021); https://doi.org/10.1007/s10854-021-06360-0
9. X. Liu, S. Cheng, H. Liu, S. Hu, D. Zhang, and H. Ning, *Sensors*, **12**, No. 7: 9635 (2012); https://doi.org/10.3390/s120709635
10. P. Biswas, C. Zhang, Y. Chen, Z. Liu, S. Vaziri, W. Zhou, and Y. Sun, *Biosensors*, **11**, No. 9: 326 (2021); https://doi.org/10.3390/bios11090326
11. S. Zampolli, I. Elmi, G. C. Cardinali, L. Masini, F. Bonafè, and F. Zardi, *Sensors and Actuators B: Chemical*, **305**, No. 8: 1274 (2020); https://doi.org/10.1016/j.snb.2019.127444
12. M. I. A. Asri, M. N. Hasan, M. R. A. Fuaad, Y. M. Yunos, and

M. S. M. Ali, *IEEE Sensors Journal*, **2**, No. 17: 18381 (2021); https://doi.org/10.1109/JSEN.2021.3091854
13. H. Xu, P. Wu, C. Zhu, A. Elbaz, and Z. Z. Gu, *Journal of Materials Chemistry C*, **1**, No. 38: 6087 (2013); https://doi.org/10.1039/C3TC30722K
14. R. Yu, Y. Chen, L. Shui, and L. Xiao, *Sensors*, **20**, No. 10: 2996 (2020); https://doi.org/10.3390/s20102996
15. M. Aazi, M. Kudinova, D. Kinet, J. L. Auguste, S. Delépine-Lesoille, P. Mégret, and G. Humbert, *Journal of Physics: Photonics*, **2**, No. 1: 014005 (2019); https://doi.org/10.1088/2515-7647/ab5cec
16. J. Li, H. Yan, H. Dang, and F. Meng, *Optics & Laser Technology*, **135**: 106658 (2021); https://doi.org/10.1016/j.optlastec.2020.106658
17. Y. Zhang, C. Wang, L. Zhao, F. Liu, X. Sun, X. Hu, and G. Lu, *Sensors and Actuators B: Chemical*, **334**: 129514 (2021); https://doi.org/10.1016/j.snb.2021.129514
18. H. Wang, Y. Luo, B. Liu, L. Gao, and G. Duan, *Sensors and Actuators B: Chemical*, **338**: 129806 (2021); https://doi.org/10.1016/j.snb.2021.129806
19. M. Wang, Y. Zhu, Q. Luo, C. Ge, G. Liu, G. Qiao, and E. G. Kim, *Applied Surface Science*, **566**: 150750 (2021); https://doi.org/10.1016/j.apsusc.2021.150750
20. Y. Wang, Y. Cui, X. Meng, Z. Zhang, and J. Cao, *Surfaces and Interfaces*, **24**: 10110 (2021); https://doi.org/10.1016/j.surfin.2021.101110
21. K. Karthik, S. Dhanuskodi, C. Gobinath, and S. Sivaramakrishnan, *Spectrochimica Acta Part A: Molecular and Biomolecular Spectroscopy*, **139**: 7 (2015); https://doi.org/10.1016/j.saa.2014.11.079
22. J. K. Rajput, T. K. Pathak, V. Kumar, H. C. Swart, and L. P. Purohit, *Physica B: Condensed Matter*, **535**: 314 (2018); https://doi.org/10.1016/j.physb.2017.08.014
23. J. C. Boettger, *International Journal of Quantum Chemistry*, **107**, No. 15: 2988 (2007); https://doi.org/10.1002/qua.21350
24. H. P. Singh and B. Dayal, *Solid State Communications*, **7**, No. 10: 725 (1969); https://doi.org/10.1016/0038-1098(69)90651-6
25. Joseph A. Spencer, Alyssa L. Mock, Alan G. Jacobs, Mathias Schubert, Yuhao Zhang, and Marko J. Tadjer, *Applied Physics Reviews*, **9**, No. 1: 2113 (2022); doi:10.1063/5.0078037
26. K. A. Jasim, T. J. ALwan, K. H. Mahdi, and H. L. Mansour, *Turkish Journal of Physics*, **37**, No. 2: 237 (2013); doi:10.3906/fiz-1203-16
27. E. Sirotin and M. Shaskolskaya, *Fundamentals of Crystal Physics* (Moskva: Mir: 1982) (in Russian).
28. R. A. Al-Ansari, H. Q. Khaleel, J. H. Awadh, G. H. Mohammed, and I. R. Swadi, *DJPS*, **13**, No. 4: 91 (2017); http://dx.doi.org/10.24237/djps.1304.318E
29. Y. S. Ocak, D. Batibay, and S. Baturay, *Journal of Materials Science: Materials in Electronics,* **29**, No. 20: 17425 (2018); https://doi.org/10.1007/s10854-018-9841-2
30. S. Dugan, M. M. Koç, and B. Coşkun, *Journal of Molecular Structure*, **1202**: 127235 (2020); https://doi.org/10.1016/j.molstruc.2019.127235
31. R. A. Moqbel, M. A. Gondal, T. F. Qahtan, and M. A. Dastageer, *International Journal of Energy Research*, **42**, No. 4: 1487 (2018); https://doi.org/10.1002/er.3935

32. Y. Lin, W. J. Wang, J. Cai, M. Ying, R. Zhao, M. Li, and N. Ce-Wen, *Phys. Rev. B*, **73**: 193308 (2006); https://doi.org/10.1103/PhysRevB.73.193308
33. J. J. Shea, *IEEE Electrical Insulation Magazine*, **21**, No. 4: 57 (2005); https://doi.org/10.1109/MEI.2005.1490003
34. A. A. Yousif and M. H. Hasan, *J. Biosens. Bioelectron*, **6**, No. 4: 254 (2015); https://doi.10.4172/2155-6210.1000192
35. A. Sreedhar, M. Hari Prasad Reddy, S. Uthanna, and J. F. Pierson, *International Scholarly Research Notices*, **1**: 527341 (2013); https://doi.org/10.1155/2013/527341
36. J. A. Dirksen, K. Duval, and T. A. Ring, *Sensors and Actuators B: Chemical*, **80**, No. 2: 125 (2001); https://doi.org/10.1016/S0925-4005(01)00898